RESEARCH ARTICLE

NANO · MICRO small
www.small-journal.com

On the Low-Pressure Hysteresis (LPH) in Gas Sorption Isotherms of Porous Carbons

Tomáš Zelenka, Lucie Zelená, Coset Abreu-Jaureguí, Joaquin Silvestre-Albero, Gabriela Zelenková, and Václav Slovák*

This study investigates the origin of low-pressure hysteresis (LPH) in the adsorption and desorption of three different probe molecules: carbon dioxide, nitrogen, and argon, across various adsorption temperatures (from cryogenic to room temperature), and within five different carbon materials: synthetic carbons (pristine and one post-synthetically oxidized) and natural coal. Significant attention is dedicated to elucidating LPH in oxidized samples outgassed at various temperatures (120–350 °C). Experimental results show that insufficient outgassing temperature can lead to unreliable data due to artificial LPH and significantly underestimated textural properties, primarily caused by porosity blockage from substances like moisture. Conversely, in samples where heteroatoms have a stabilizing effect on texture, such as natural coal, careful consideration of outgassing temperature is crucial due to the risk of thermal degradation. Other factors contributing to LPH are adsorption temperature, and especially, kinetic limitations at cryogenic temperatures for cellulose-based carbons. Minor factors responsible for LPH are the physical state of the sample (monolith vs powder) and the flexibility of the porous system, both studied by carbon dioxide sorption. This study constitutes an important piece in the evaluation of LPH, providing practical recommendations and underlining the importance of experimental design, with implications for further research in this complex field.

1. Introduction

Hysteresis loops are a common occurrence during the adsorption–desorption process of gases in mesoporous solids and are usually associated with the metastability of the fluid and/or network effects. In the specific case of micropores and small mesopores with diameters below ca. 4 nm, the adsorption–desorption of nitrogen at −196 °C or argon at −186 °C is generally completely reversible.[1]

However, in certain cases, the desorption branch does not enclose the adsorption branch at relative pressures (p/p_0) below 0.42 and 0.38 for nitrogen/−196 °C and argon/−186 °C, respectively.[2] Instead, the mismatching persists, and an extended hysteresis loop appears, commonly referred to as a *low-pressure hysteresis* (*LPH*), *artificial hysteresis*, or *open isotherm*. LPH has been observed or studied in various porous materials, particularly those with narrow micropores, such as zeolites, MOF materials, activated carbons, or porous glasses. When utilizing adsorption–desorption isotherms that involve LPH for texture characterization, caution is advised during the calculation and interpretation of results, as these may prove to be non-reproducible and unreliable.[3,4]

Table 1 summarizes potential factors contributing to the occurrence of LPH. For carbon materials, genuine (true) LPH is often attributed to volumetric changes – contractions and expansions – of the samples' porous structure caused by adsorption-induced deformation, particularly in non-rigid structures.[5,6] Non-genuine (artificial) LPH often stems from a lack of equilibration or insufficient outgassing conditions, both of which can be mitigated by the operator by optimizing experimental conditions.[7]

The situation becomes more problematic for some ultramicroporous materials. Due to the presence of narrow constrictions, a true equilibrium can hardly be achieved in a reasonable time interval. The presence of diffusional restrictions (kinetic limitations), maximized under cryogenic temperature conditions, prevents the proper characterization of the porous structure.[16] For that reason, CO_2 adsorption at an elevated temperature of 0 °C is often recommended to overcome diffusion limitations, though these limitations might persist even at a higher temperature.[17]

T. Zelenka, L. Zelená, G. Zelenková, V. Slovák
Department of Chemistry, Faculty of Science
University of Ostrava
30. dubna 22, Ostrava CZ-702 00, Czech Republic
E-mail: tomas.zelenka@osu.cz

L. Zelená
Department of Inorganic Chemistry
Faculty of Science
P. J. Šafárik University
Moyzesova 11, Košice SK-041 01, Slovak Republic

C. Abreu-Jaureguí, J. Silvestre-Albero
Laboratorio de Materiales Avanzados
Departamento de Química Inorgánica-Instituto Universitario de Materiales
Universidad de Alicante
San Vicente del Raspeig E-03690, Spain

The ORCID identification number(s) for the author(s) of this article can be found under https://doi.org/10.1002/smll.202311990

DOI: 10.1002/smll.202311990

Table 1. Summary of possible reasons for LPH for various samples.

Possible responsible aspect of LPH	Studied samples	Genuine/Non-genuine LPH
A structural flexibility, expansion, and contractions (volumetric changes) of the sample during adsorption and desorption.	carbon,[3,8,9] MOF[10–12]	Genuine
A rearrangement of adsorbed molecules.	zeolite,[13] porous glasses[14]	Genuine
A lack of equilibration during adsorption–desorption experiment and/or diffusion restrictions.	carbon,[7] silica,[7] MOF[15]	Non-genuine
An insufficient outgassing of the sample.	carbon[7]	Non-genuine

The overlooked diffusion limitations during the assessment of textural properties through gas physisorption could result in fundamentally flawed conclusions, impacting the reliability of research outcomes. Some of our recent experimental results align with this observation, although they may also be associated with other above-mentioned factors, such as the flexibility of the material, among others. While LPH has been investigated within the context of outgassing conditions, our current understanding does not include the impact of outgassing temperature on post-synthetically modified (oxidized) samples or natural samples containing inherent oxygen-functional groups in their structure with respect to LPH.

With these premises, our paper aims to enhance the understanding of the low-pressure hysteresis (LPH), an important aspect often overshadowed by the broader challenges of material characterization, through the systematical and careful evaluation of five different case studies: as-synthesized and post-synthetically oxidized resorcinol-formaldehyde-based carbon – STR, as-synthesized cellulose-based carbons – CMG, and natural coal. These model systems are characterized by a different raw material, a different porous structure, and important differences in chemical properties. Significant attention is dedicated to the quantification of LPH by employing the *extent of LPH* parameters and elucidating the LPH in samples with modified surface chemistry (oxidized samples). We also explored the LPH phenomenon in relation to various factors such as the physical state of the sample (powder vs pieces), adsorptive and adsorption temperature, outgassing temperature, the flexibility of the porous system, and potential kinetic limitations during the sorption experiment. This comprehensive and systematic approach enhances the understanding of the causes behind LPH, which is crucial for its mitigation. Moreover, our study elucidates the impact of inappropriate outgassing conditions not only on LPH but also on the overall calculated textural properties of materials affected by LPH.

2. Results and Discussion

The first steps of this study focused on evaluating the effect of particle morphology (Section 2.1.), adsorption temperature (Section 2.2.), and outgassing conditions (Section 2.3.) on the nature and extent of the LPH. These experiments were performed using the pristine and post-synthetically oxidized STR resorcinol-formaldehyde-based carbon (STR, STR-ox). For comparative purposes, natural coal will be added in the final Section 2.3. devoted to highlighting challenges in removing substances that block the porosity, reduce LPH, and preserve the sample's texture. The main goal is to identify optimal outgassing conditions for samples with oxygen functionalities occurring naturally (coal) and those introduced post-synthetically (STR-ox).

2.1. LPH and Physical State of the Sample

The presence of an LPH may be influenced by the particle size of the sample.[14] To evaluate this effect, we conducted CO_2/25 °C sorption analysis in the oxidized STR sample in two different physical states: as-prepared monolith (binder-free pellet) and

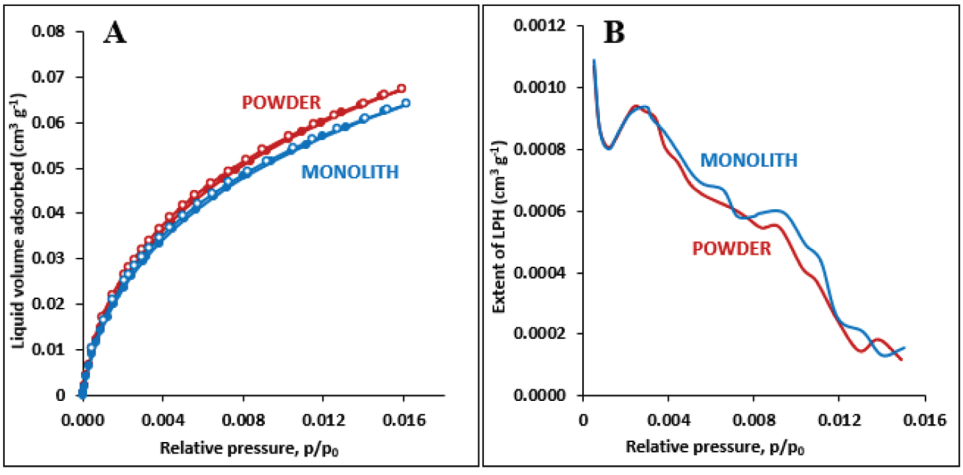

Figure 1. CO_2/25 °C adsorption and desorption isotherms a) and the extent of LPH b) for the oxidized STR sample in monolithic and powdered form.

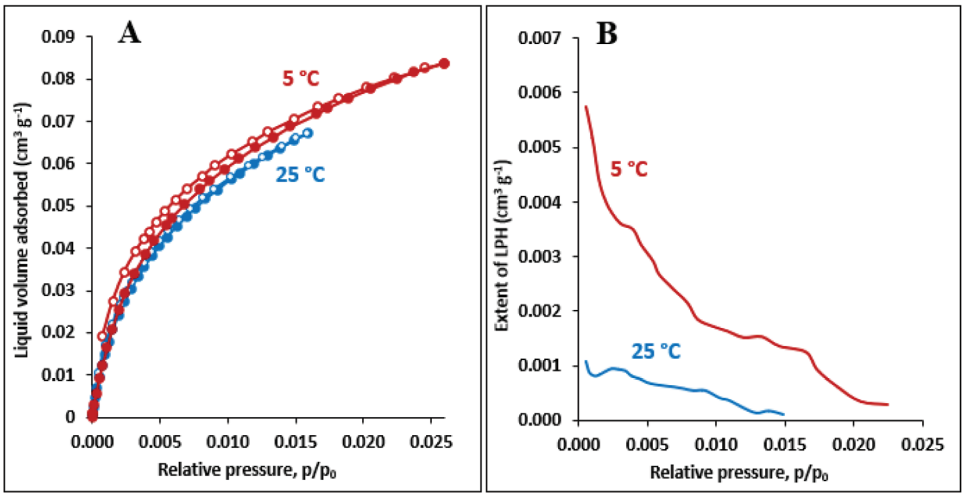

Figure 2. Adsorption–desorption isotherms of CO_2 at 5 and 25 °C a) and corresponding extents of LPH b) for the oxidized STR sample.

its powdered form, both outgassed at 120 °C. CO_2 adsorption–desorption isotherms (**Figure 1a**) show a slightly higher (by ca. 5%) adsorption capacity for powdered sample over the monolithic one, which may be related to the possible formation of additional microporosity and/or enhanced pore accessibility as a result of the fragmentation of the sample. However, the extent of LPH (Figure 1b) remains unchanged regardless of the sample morphology, which allows us to conclude that the extent of LPH is not related to the physical state of the sample (for the given system and experimental conditions). Therefore, to facilitate comparison, we conducted the remaining gas sorption measurements exclusively on powdered samples.

2.2. LPH and Adsorption Temperature

It is known that LPH can be influenced by the adsorption temperature.[10] For that reason, we performed CO_2 sorption experiments at 5 and 25 °C on the oxidized STR sample, outgassed at 120 °C.

Figure 2a displays CO_2 sorption isotherms where the adsorbed volume is presented in the liquid state. The conversion of the amount adsorbed to cm^3(liquid) g^{-1} serves to normalize it by the liquid density of the probe gas within the pores at a specific temperature. This normalization follows the Gurvich rule[18] that assumes that fluid adsorbed in the pores has the same density as the bulk liquid at the same temperature and pressure.[19] This method of normalization helps us to more clearly identify changes in adsorbed volume that result from kinetic restrictions. Since the sample adsorbs slightly more at 5 °C than at the higher temperature of 25 °C, we speculate that the minor difference is not due to CO_2 accessibility/kinetics limitations. To make sure that all the measurements were properly equilibrated, analysis of kinetic curves was performed for low, medium, and high relative pressure points (Figure S1, Supporting Information). All the points that have been chosen for equilibrium analysis can be regarded as reasonably equilibrated. However, the possibility that improper equilibration may account for this minor difference in adsorbed volumes at 5 and 25 °C cannot be dismissed.

When considering LPH, a significant decrease in the extent of LPH becomes evident when the experimental temperature is raised by 20 °C (Figure 2b). A similar trend was observed in ref., [10] where authors investigated CO_2 adsorption hysteresis in ultramicroporous Metal-Organic Framework (MOF) materials, identifying adsorption temperature as one of the factors influencing hysteresis. In summary, adsorption temperature affects the extent of LPH so it decreases with increasing adsorption temperature. This observation aligns perfectly with the concept that kinetic limitations are minimized at higher adsorption temperatures.

2.3. LPH and Outgassing Temperature

It is widely recognized that conducting a proper outgassing process on the sample before performing adsorption measurements is essential. This step ensures the thorough cleaning of the material's surface, enabling the acquisition of reproducible and reliable data.[1,16] The effect of outgassing temperature on LPH was monitored by N_2/−196 °C sorption on the oxidized STR sample that had been pre-outgassed at different temperatures, ranging from 120 to 350 °C.

Obtained adsorption–desorption isotherms and calculated extents of LPH are illustrated in **Figure 3a–c**, respectively. It is clear that the extent of LPH decreases significantly (6 times, calculated for 0.4 p/p_0) if the outgassing temperature increases from 120 to 350 °C (Figure 3b,c). Such a trend is in agreement with the results of the study by Silvestre-Albero et al.,[7] where the authors found that a drying temperature of 150 °C (for 4 h) was probably insufficient to properly clean the surface of the measured activated carbons. This is also suggested by our results, where an increase in the outgassing temperature from 120 to 350 °C increases the adsorbed volume (by 4.6 times, calculated for 0.99 p/p_0), pore size distributions (Figure 3d), and calculated textural properties, where the micropore volume increased 41 times and the mesopore volume 3.3 times (**Table 2**). Mesoporosity is usually related to the presence of a hysteresis loop, which has a different shape for 120 °C compared to higher outgassing

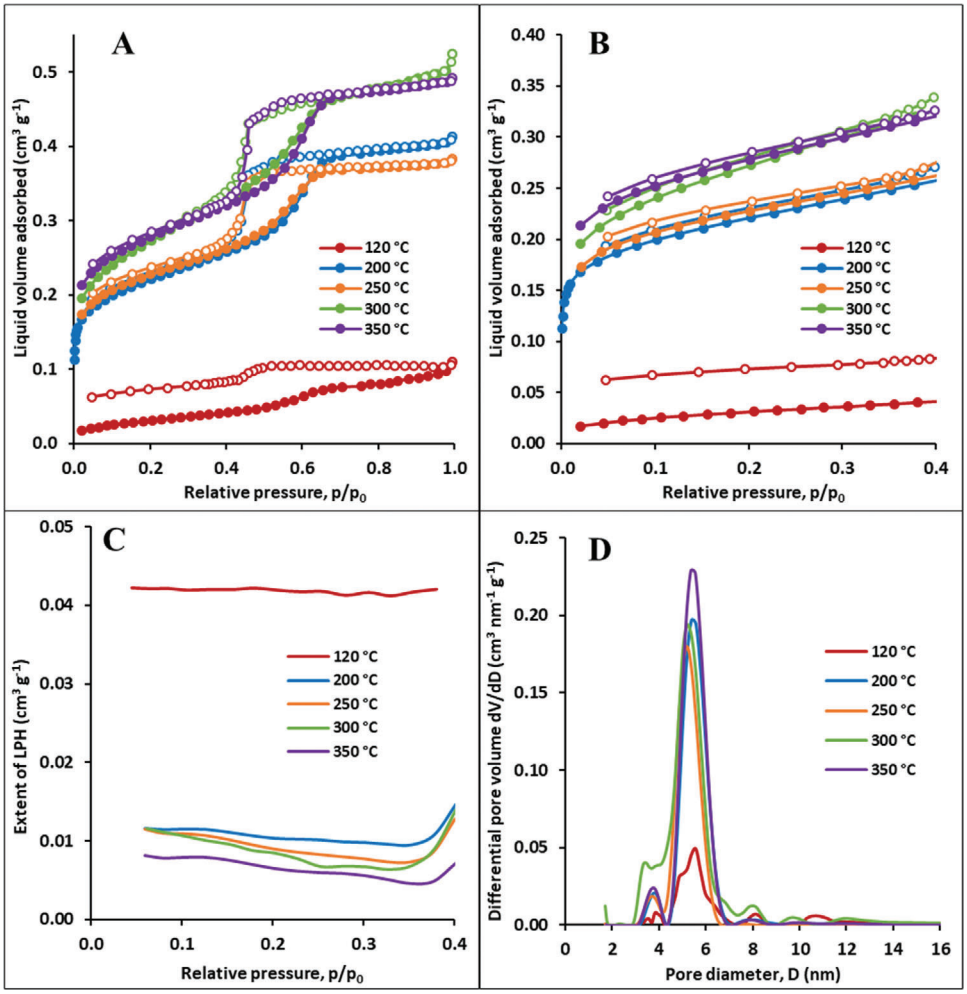

Figure 3. N_2/−196 °C adsorption and desorption isotherms a), their low-pressure part b), the extents of LPH c), and pore size distributions d) for the oxidized STR sample (STR-ox) outgassed at different temperatures.

temperatures. Microporosity is then represented by a knee on the isotherm roughly below 0.1 p/p_0, and is absent at 120 °C. It can be summarized that texture, such as micro- and mesoporosity is notably influenced by outgassing conditions, especially between 120 and 200 °C, where micropore volume increased from 0.004 to 0.122 $cm^3\ g^{-1}$ (Table 2) and LPH was reduced 4.4 times.

Based on the performed experiments on the oxidized STR sample, it is clear that reliable isotherms (with acceptable LPH) and derived textural parameters require proper outgassing conditions (an outgassing temperature high enough to completely remove substances like moisture, here, 300 or 350 °C). As a result, pore size distributions and the resulting textural parameters are reliable only when the optimum outgassing temperature is reached, lower outgassing temperatures provide misleading textural details.

Table 2. The volume of micropores and mesopores (V_{micro}, V_{meso}) obtained by N_2/−196 °C sorption on the oxidized STR sample outgassed at different temperatures.

Outgas temperature of oxidized STR	V_{micro} [$cm^3\ g^{-1}$]	V_{meso} [$cm^3\ g^{-1}$]
120 °C	0.004	0.088
200 °C	0.122	0.261
250 °C	0.138	0.218
300 °C	0.142	0.333
350 °C	0.165	0.294

To investigate the reason for the decreasing LPH with higher outgassing temperature, it is necessary to consider the nature of the sample's surface. Since the STR is a post-synthetically oxidized material, it can be assumed that all the functional groups (heteroatoms) are bound to the pore surface. These heteroatoms may be responsible for enhanced interactions with water molecules, whether they come from the ambient air or persist within the sample after being washed with water following oxidation. The water or other substances may remain trapped in the porous system due to the low outgassing temperature. As a result, the pore capacity at the level of micropores as well as mesopores may be reduced. An outgassing temperature of 200 °C is probably responsible for removing most substances from mesopores but is not high enough to completely make the porosity accessible for gas sorption. Thus, an increase in

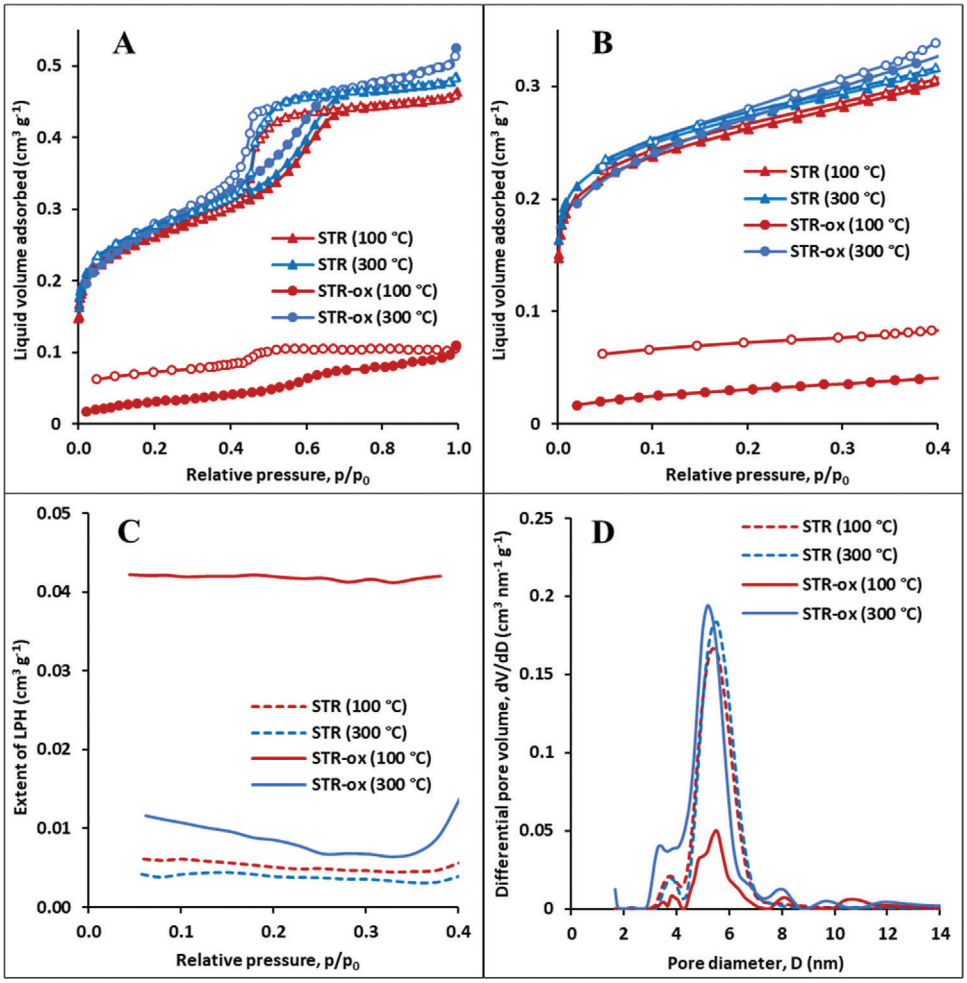

Figure 4. N_2/−196 °C adsorption–desorption isotherms a), their low-pressure part b), the extents of LPH c), and pore size distributions d) for the non-oxidized STR sample outgassed at 100 and 300 °C. The STR-ox represents the oxidized STR sample.

drying temperature is required to eliminate as many adsorbed substances from the material as possible.

To confirm if the retention of adsorbed substances (e.g., water molecules) is somehow related to the oxidized surface of the material, N_2/−196 °C sorption measurements on the pristine (non-oxidized = containing a minimal quantity of surface functionalities) STR sample were performed with the use of the outgassing temperatures of 100 and 300 °C. Recall that in the case of the oxidized sample, notable differences were observed in the isotherms, as well as the derived textural parameters and the extent of LPH when the sample underwent outgassing at 120 °C and 300 °C (Figure 3 and Table 2). However, when examining **Figure** 4a–d and **Table** 3 for the pristine sample, it is evident that the volume of micropores or mesopores did not exceed a 6% increase at 300 °C compared to the 100 °C outgassing temperature. Similarly, minimal variations were observed in the extent of LPH when the samples underwent outgassing at 100 or 300 °C. The consistent behavior observed in the pristine sample, regardless of the outgassing temperature, supports our hypothesis that the presence of an LPH in oxidized STR can be attributed to the heteroatoms present on its pore surface.

To obtain information about the oxygen content of the samples, which is the most expected heteroatom in oxidized samples, XPS analysis was performed after each of these thermal treatments. The oxygen and carbon atomic percentages are summarized in **Figure** 5, and XPS spectra are shown in Figure S2 (Supporting Information). Figure 5 reveals that the pristine STR sample is found to have an oxygen content of 9.3 at.%, while the oxidized STR sample shows a notably higher oxygen content of 22.9 at.%. This discrepancy amounts to 13.6 at.% is a result of the oxidation process applied to the STR sample. For the STR-ox samples that underwent pre-outgassing at progressively higher

Table 3. The volume of micropores and mesopores (V_{micro}, V_{meso}) obtained by N_2/−196 °C sorption on the pristine (non-oxidized) STR sample outgassed at 100 and 300 °C.

Outgas temperature of STR	V_{micro} [$cm^3\ g^{-1}$]	V_{meso} [$cm^3\ g^{-1}$]
100 °C	0.156	0.274
300 °C	0.165	0.286

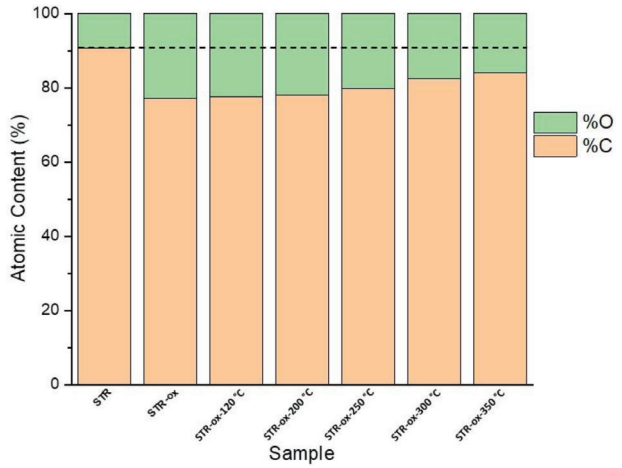

Figure 5. The percentage atomic content of carbon and oxygen atoms in the pristine STR sample, non-outgassed oxidized STR (STR-ox) sample, and its derivatives were outgassed from 120 to 350 °C. The dashed line represents the oxygen content of the pristine STR sample. Data derived by XPS.

temperatures in a vacuum (in a physisorption analyzer), a reduction in the oxygen content was observed, particularly when the pre-outgassing temperature exceeded 200 °C. At the highest outgassing temperature of 350 °C, the sample still contains 16.0 at.% of oxygen, which is ≈6.7 at.% more oxygen than the pristine STR sample. The reduction of oxygen content on the pore walls (which is probably responsible for retentions of substances such as moisture) as the outgassing temperature increases is probably the underlying reason for the decrease in the extent of LPH, as indicated in Figure 3c. Samples outgassed at 300 and 350 °C exhibited an acceptable level of LPH, with oxygen contents of 17.6 at.% and 16.0 at.%, respectively.

The samples that underwent XPS analysis were also analyzed by TG-MS technique to identify the gases being released from the samples during the outgassing procedure. First, the results from TG-MS analysis of non-outgassed samples (pristine STR, STR-ox) are illustrated in Figure S3a,b (Supporting Information). The pristine STR exhibits a minimal mass loss of 2.7%, primarily attributed to the release of water (corresponding to the most intensive MS signals with $m/z = 18$ and 17), while the intensities of the other signals are negligible. In contrast, the oxidized STR sample lost 6 times more mass (16.4%) up to 350 °C, primarily due to the release of water, particularly up to ≈160 °C. This water is likely bound within the sample as physically trapped moisture, and it is desorbed up to this temperature. For the oxidized STR sample, it is evident that a higher quantity of physically bound water is present. This observation aligns with our hypothesis that the functional groups in the oxidized STR may contribute to retaining moisture within the porous structure of the material, particularly due to the low outgassing temperature. Beyond 160 °C, only the evolution of water and CO_2 ($m/z = 44$) was observable (CO was not detectable and thus is not shown). These products result from the decomposition of oxygen functional groups, especially carboxylic groups that decompose as CO_2 in the temperature range of ca. 200 – 450 °C. While the water evolution above 160 °C could be present from the dehydration of adjacent carboxylic groups during the sample heating.[20]

It is worth noting that we are not able to mimic well the vacuum outgassing conditions of the isotherm measurements in the TG analyzer, as the measurement takes place in a flow of inert gas (argon). For that reason, we performed TG-MS measurements for STR-ox samples ex-situ pre-outgassed in a physisorption instrument at different temperatures under a vacuum. The TG curves (Figure S4a, Supporting Information) show a clear trend, where the onset of mass loss corresponds well to the temperature at which each sample was degassed. The MS signals in Figure S4b,c (Supporting Information) correspond to the intensities of the primary gases released, i.e., water and CO_2. The signal onsets for both gases evolved over ca. 160 °C shift toward higher temperatures as the outgassing temperature was raised. The results also explain why the sample dried at 120 °C shows the highest extent of LPH and the lowest textural characteristics discussed in Figure 3 and Table 2. This is because this sample contains the largest moisture content (Figure S4b, Supporting Information) and also a significant quantity of functionalities that decomposed in the form of CO_2 (Figure S4c, Supporting Information), due to the use of a low outgassing temperature.

Based on the above results, it is evident that the reduction in adsorption capacity can be attributed to the insufficient outgassing temperature of the STR-ox sample (Figure 3a). However, there may be an additional factor contributing to the notable rise in the adsorbed volume in the low-pressure region, particularly between 250 and 300 °C (Figure 3b). The STR-ox sample contains a large number of surface oxygen groups, which were introduced by the post-treatment of the STR sample. These oxygen surface groups could lead to a decrease in pore volume within the micropores/small mesopores that are filled at this low pressure. Therefore, the increase in N_2 adsorbed volume observed between the samples STR-ox (250 °C) and STR-ox (300 °C) could essentially result from the elimination of these oxygen groups (from the pore walls or at the pore mouth) and the decomposition of the sample, as suggested by the release of CO_2 observed in the TG-MS data presented in Figures S3 and S4 (Supporting Information). To assess the contribution of these functionalities, we performed the additional experiment, where we first outgassed the STR-ox sample under the most severe outgassing temperature of 350 °C (STR-ox (350 °C)) that can be responsible for the decomposition of the surface groups. A part of the sample was used for N_2/−196 °C adsorption analysis, and a part was immersed in distilled water for 3 days to wet it again. This sample was then outgassed at 250 °C, denoted as the STR-ox (350 – 250 °C) and performed N_2/−196 °C adsorption analysis. For comparison, adsorption isotherm of the STR-ox sample outgassed at 250 °C (STR-ox (250 °C)) was measured again, too. The resulting adsorption isotherms (**Figure 6**) show that the isotherm of the sample STR-ox (350 – 250 °C) corresponds with the isotherm of STR-ox (250 °C). This explains that the increase in the adsorbed volume in Figure 3a,b between 250 and 300 °C is reversible and due to incomplete removal of pore water for STR-ox (250 °C). If the N_2 isotherm of STR-ox (350 – 250 °C) were similar to that of STR-ox (350 °C), this effect would be irreversible due to the increase in pore volume due to the decomposition of oxygen-containing groups (not the case for sample STR-ox).

To strengthen our hypothesis regarding the retention of water within the porous system due to the presence of heteroatoms and

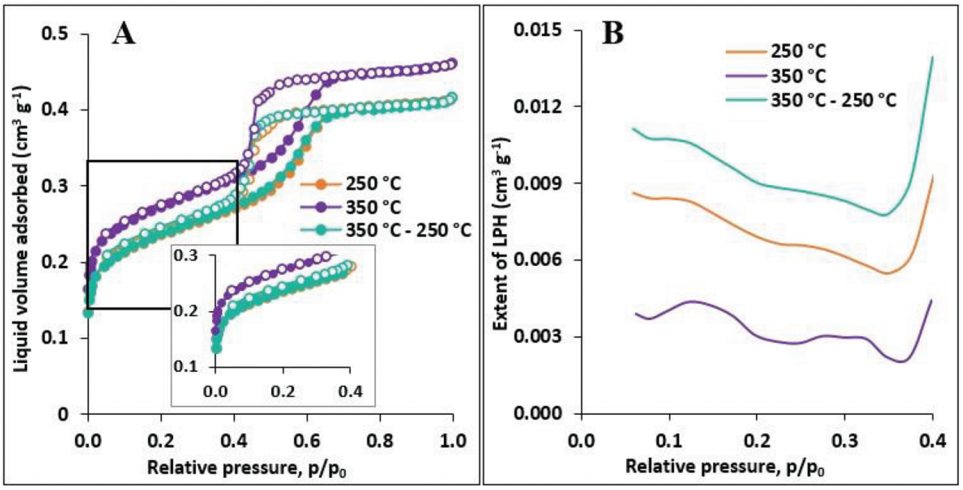

Figure 6. N_2/−196 °C adsorption and desorption isotherms including their low-pressure part in the inset a) and the extents of LPH b) for the oxidized STR sample (STR-ox) outgassed at 250 and 350 °C. The sample denoted as STR-ox (350 – 250 °C) was first outgassed at 350 °C, then wetted with distilled water, and outgassed at 250 °C prior to the sorption measurement.

their relationship with the LPH, we conducted additional testing using a lignite sample, which is a type of low-rank coal. Unlike the oxidized STR sample, heteroatoms in the lignite were not introduced post-synthetically. Instead, they naturally exist within its structure and play a role in stabilizing its gel-like (hydrogel) structure.[21] N_2/−196 °C adsorption–desorption isotherms of the lignite are shown in **Figure** 7a. The zoomed low-pressure part of the isotherms (Figure 7b) and the calculated extent of LPH (Figure 7c) show a clear decrease in LPH with increasing outgassing temperature. However, the adsorption capacity of the sample also decreases with increasing outgassing temperature, with the highest drop between temperatures of 60 and 100 °C. This trend is a long-known phenomenon observed by many authors and related to the destabilization/relaxation of its structure by removing water molecules.[22,23]

We can conclude that the post-synthetically oxidized sample requires increased temperature to clean most of its microporosity from moisture or other blocking substances. If insufficient outgassing temperature is used, at least the following issues could arise:[2,16,24,25]

i. shift of the isotherm to lower relative pressures and/or the distortion of the isotherm shape due to the quadrupolar nature of nitrogen or CO_2 adsorptive that can preferentially adsorb on heteroatoms;
ii. and/or blocking of pore entrance by substances such as moisture and other adsorbed fluids;
iii. and/or evaporation of water molecules into the manifold during the manometric gas sorption experiment, especially under low pressures.

All these scenarios then lead to unreliable raw experimental data burdened with LPH and, thus, unreliable pore sizes and other derived textural properties of analyzed samples. For this reason, we propose to use the highest possible outgassing temperature (300 or 350 °C for studied STR-ox) even at the cost of removing the surface groups (as discussed in connection with Figures 3 and 4), as long as there is no concurrent reduction in textural parameters. Certainly, when investigating thermally unstable samples, such as certain natural coals, MOFs, or

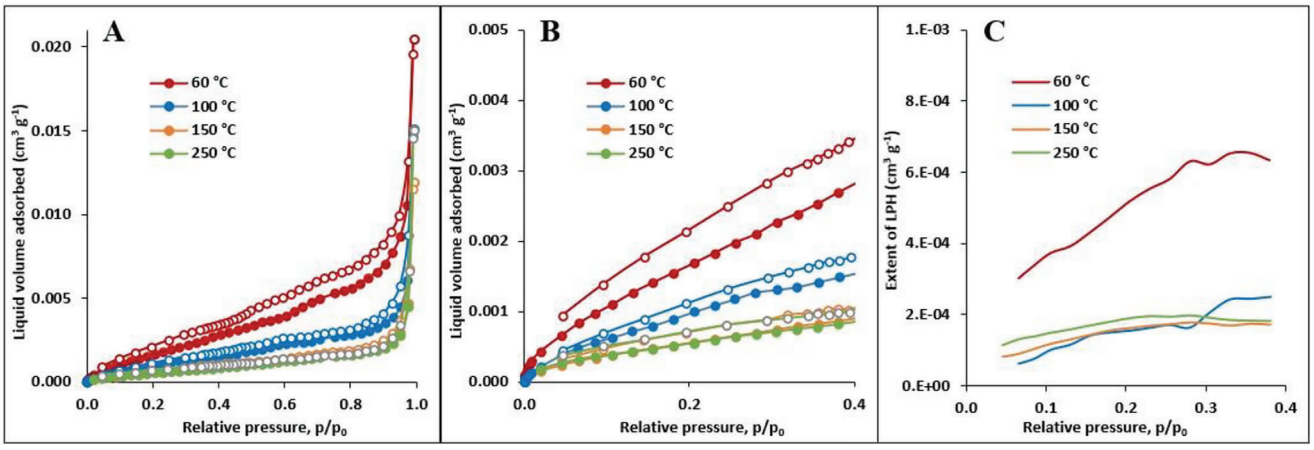

Figure 7. N_2/−196 °C adsorption–desorption isotherms a), the amplification of their low-pressure part b), and the extents of LPH c) for the lignite sample outgassed in the range of 60–250 °C.

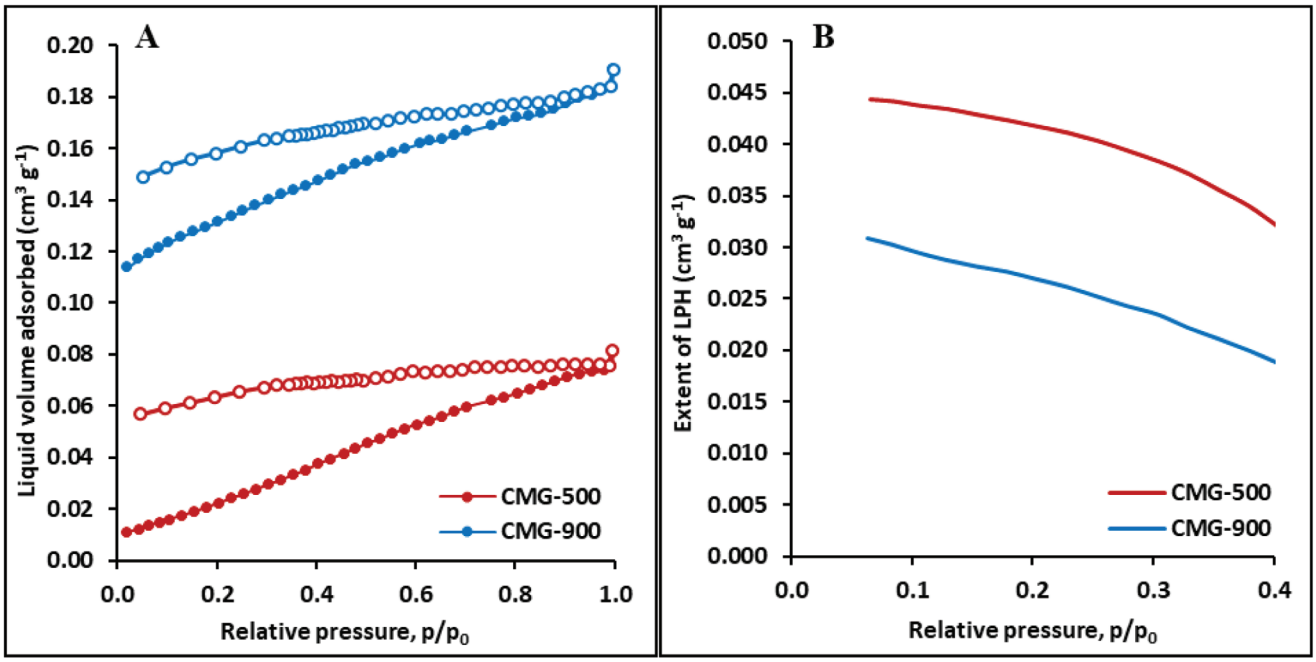

Figure 8. N_2/−196 °C adsorption–desorption isotherms a) and the extents of LPH b) of the CMG-500 and CMG-900 samples outgassed at 300 °C.

generally samples where functional groups have a structure stabilization effect, exposing them to elevated temperatures prior to sorption analysis may experience thermal degradation in their texture.[23,26,27] As a consequence, the calculated textural parameters may not accurately reflect the real characteristics of the material. Hence, it is crucial to determine an optimal drying temperature where the texture of the sample remains stable, for example by conducting a series of adsorption measurements with progressively elevated outgassing temperatures, carefully monitoring reduction in textural parameters, and, if possible, employing another analysis method such as TG-MS or XPS. We also propose, especially for treated (e.g., oxidized) samples, performing the experiment related to Figure 6 consisting of outgassing – wetting – re-outgassing. It appears evident that, for certain samples, obtaining genuine textural characteristics through gas sorption is challenging. The decision to outgas at lower temperatures, posing the risk of underestimating textural parameters, or at higher temperatures, with the potential of altering texture, presents a dilemma that requires thoughtful consideration. Further research in this field is worthwhile.

The presented results demonstrate a beneficial effect of higher outgassing temperatures in reducing LPH across all the samples – STR (both, oxidized and pristine, Figures 3 and 4), and lignite (Figure 7). Therefore, we expected that the same scenario would apply also to CMG samples, where cellulose served as another carbon precursor. These as-synthesized samples, differing from each other only by pyrolysis (carbonization) temperature of 500 °C vs 900 °C (denoted as CMG-500 and CMG-900, respectively), were tested in their as-synthesized form, i.e., without undergoing any post-synthetic oxidation process. Therefore, based on the insights gained from STR samples, an outgassing temperature of 300 °C was expected to minimize the extent of LPH. Unfortunately, N_2/−196 °C isotherms showed significant LPH for both CMG carbons (**Figure** 8a,b), despite the high temperature applied in the outgassing treatment. It is worth noting that the carbon produced by the higher pyrolysis temperature had larger microporosity (micropore volume = 0.100 cm^3 g^{-1}), while the lower pyrolysis temperature produced carbon with low or inaccessible microporosity to nitrogen molecules at −196 °C (micropore volume = 0.000 cm^3 g^{-1}). The volume of mesopores was comparable for both samples, 0.071 and 0.073 cm^3 g^{-1}.

Carbons are known for their flexible porosity, which can result in volumetric changes during adsorption–desorption experiments,[3,8,9] and can be a reason for persisting LPH. In the next section of this study, the effect of structural flexibility in the LPH will be evaluated for these cellulose-based samples (CMG samples), comparing them with the STR-ox sample as a reference where no flexibility is expected.

2.4. LPH and Flexibility of Samples

The LPH was also observed in cellulose-based carbons upon tetrachloride vapor sorption at 20 °C and the authors attributed it to expansion resulting from the intercalation of tetrachloride molecules in micropores.[28] To investigate the flexibility of the porous structure in CMG samples, thermomechanical analysis (TMA) was employed. For this purpose, CO_2 sorption measurements at the adsorption temperature of 15 °C (the lowest achievable stable temperature on the instrument) were performed. In addition to CMG samples, the oxidized STR sample was also used as a reference. **Figure 9** displays thermomechanical curves indicating the expansion of the samples resulting from the sorption of CO_2 within a time range of 120 to 180 min. The results demonstrate that the flexibility of all samples is low and well reversible, as the expansion induced by CO_2 sorption is below 0.07% for each sample. Surprisingly, cellulose-based carbons (CMG-500 and 900) exhibit lower expansion compared to the STR-ox reference. These results suggest that the presence of LPH

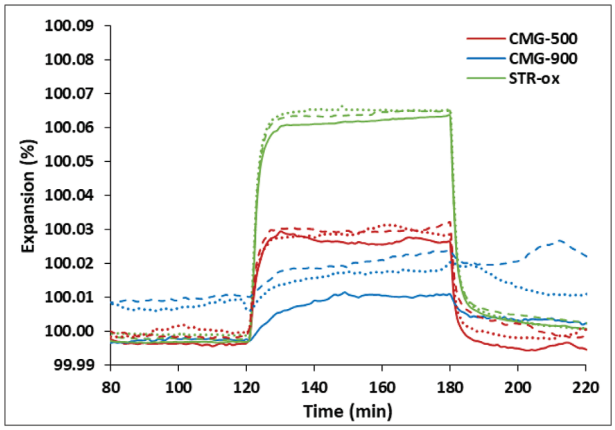

Figure 9. Expansion of the STR and CMG samples during CO_2/15 °C sorption (time = 120 – 180 min) obtained by TMA analysis. STR-ox represents an oxidized STR sample. Three different types of lines represent three independent measurements. Be aware that the *x*-axis does not originate from zero.

in these cellulose-based CMG samples is probably not related to the flexibility of the material during CO_2 sorption, as expected. To find the underlying reason for the persistent LPH, we decided to investigate it in the context of potential kinetic restrictions (diffusion limitations), a phenomenon commonly observed in carbon materials.

2.5. LPH and Kinetic Limitations of Gas Sorption

To determine the cause of LPH in CMG samples, gas sorption measurements were performed at two different adsorption temperatures, i.e., −186 and −196 °C, and using a rather "inert" probe molecule, such as Ar (a spherical molecule with no quadrupole moment). Generally, when diffusion limitations are absent, the amount physisorbed decreases with increasing adsorption temperature.[29] Our Ar isotherms show an opposite trend for the CMG-500 (**Figure 10a**) as well as the CMG-900 (Figure 10c) sample. This proves our hypothesis about the kinetic limitations that may play a key role during gas sorption measurements, at least at cryogenic temperatures where gas accessibility to pores of molecular sizes (ultramicropores) is restricted. A more detailed examination of the adsorption isotherm shapes at each temperature reveals important distinctions. At −186 °C, both samples exhibited a rounded knee at low relative pressures on the adsorption branch, suggesting potential filling of micropores. However, the adsorption branch was more linear in shape at −196 °C, which further supports our diffusion limitation theory. This trend was particularly evident for CMG-500, showing minimal adsorption at −196 °C and low pressures. Significant kinetic restrictions are also well seen during the desorption of argon molecules from the CMG-500 sample (for both −196 and −186 °C). Horizontal desorption branches indicated that all the argon molecules remained completely adsorbed/trapped within the pores without undergoing any desorption. This sample showed large LPH, as demonstrated by the extent of LPH (Figure 10b). Partial desorption and a significantly lower extent of LPH can be seen for the sample CMG-900, probably due to the developed narrow mesoporosity as demonstrated by regular (high-pressure) hysteresis accompanied by the partial closure of the regular hysteresis loop (Figure 10c,d).

Determining porous properties from argon adsorption, particularly at −196 °C is very difficult. The challenge arises from the fact that only the equilibrium DFT kernel is available for Ar adsorption at −196 °C, which produces artificial pore size distributions when applied to isotherms containing low-pressure hysteresis.[4] Therefore, **Table 4** does not include porous parameters for Ar/−196 °C. Instead, it presents data only for Ar/−186 °C and N_2/−196 °C, assuming cylindrical pore geometry for comparative purposes. This choice arises from the unavailability of the hybrid slit/cylindrical QSDFT adsorption kernel for the Ar/−186 °C isotherm in the employed software. To mitigate the impact of the calculation model on textural property outcomes, we approximate the micropore volume using the volume of liquid adsorbed at 0.1 p/p_0 ($V_{0.1}$) and the sum of micropore and partially mesopore volumes using $V_{0.85}$ (volume adsorbed at 0.85 p/p_0). The partial volume of mesopores is estimated by $V_{0.85\text{-}0.1}$ (Table 4). All three parameters exhibited substantial increases by hundreds of percent, ranging from ≈159% to 373% when Ar adsorption for CMG-500 was conducted at a temperature 10 °C higher compared to −196 °C. The most notable difference was observed for the $V_{0.1}$ parameter, approximating micropore volume. This aligns perfectly with our hypothesis regarding strong kinetic limitations for nitrogen to access the CMG-500 sample. For the CMG-900 sample, kinetic constraints appear to be relatively mild, as the parameters are higher by ≈9% to 18% when a higher Ar adsorption temperature is used. Ar/−186 °C isotherms can therefore be considered more reliable than those obtained at −196 °C. By comparing the results from Ar/−186 °C adsorption with N_2/−196 °C, it is evident that parameters from the Ar isotherm are generally higher, with larger differences observed for CMG-500 and minor differences for CMG-900. This underscores the Ar/−186 °C method as the most reliable under cryogenic temperature conditions.[30] Therefore, calculated microporous and mesoporous volumes ($V_{micro,}$ V_{meso} in Table 4) should be considered unreliable for N_2/−196 °C.

Due to the diffusion limitations for gases under cryogenic conditions, resulting in their restricted access to fine pores, we conducted CO_2 adsorption experiments at elevated temperatures of 25 and 40 °C on the CMG samples. Since 40 °C is supercritical temperature for CO_2 at 101 kPa, the amount of CO_2 adsorbed cannot be recalculated to the liquid state. Consequently, the isotherms (**Figure 11a,c**) fail to offer insights into potential diffusion limitations. Instead, our focus shifts to kinetic records. Figures S5 and S6 (Supporting Information) illustrate kinetic records, with normalized pressure coordination covering the whole range of the isotherm (3 – ca. 90 kPa) for the CMG-500 and the CMG-900 samples, respectively. Generally, desorption processes achieve equilibrium rapidly, usually within 10 – 30 min at both temperatures for both samples. Pressure fluctuations are observable during supercritical desorption measurements conducted at 40 °C. Adsorption proves to be a controlling process due to its prolonged equilibration (20 – 60 min), indicating the presence of kinetic restrictions. Nevertheless, desorption also contributes to the limitations as molecules are trapped in the porous network and delay the desorption. These restrictions may be a key factor contributing to the persistence of LPH despite elevated measurement temperatures.

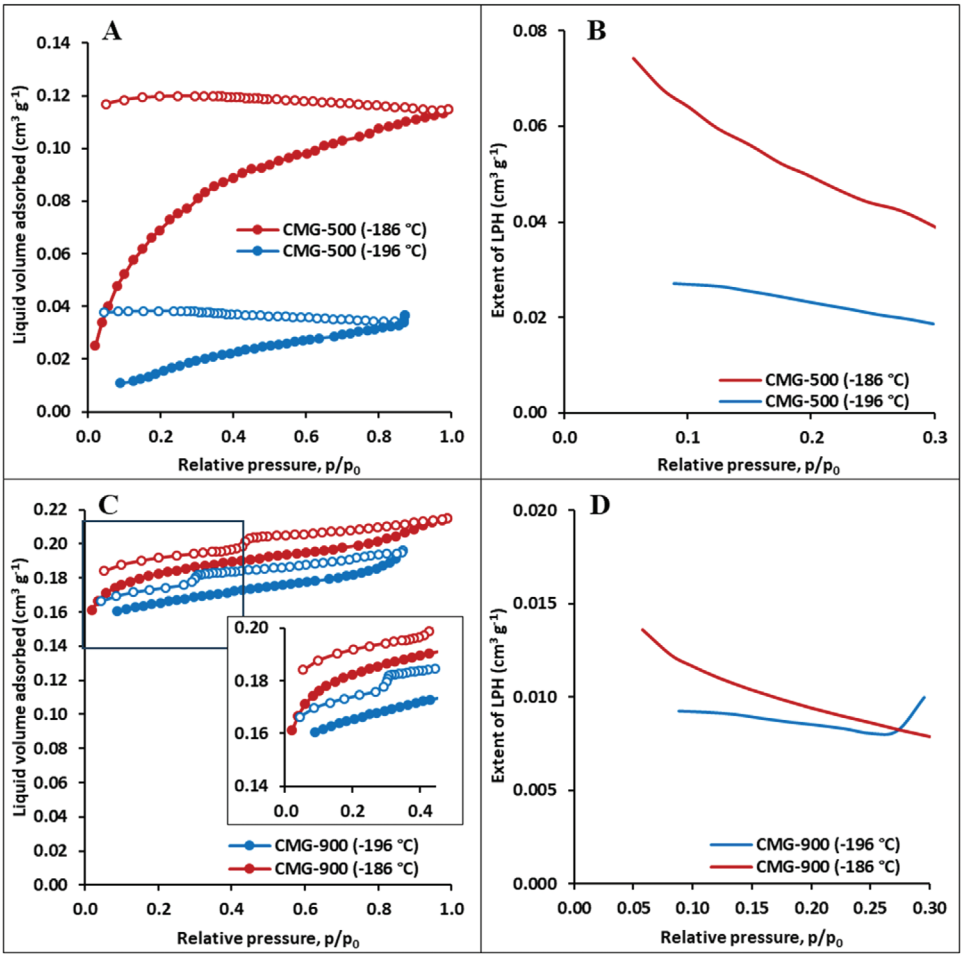

Figure 10. Ar adsorption–desorption isotherms obtained at −196 and −186 °C a,c), corresponding extents of LPH b,d) for the CMG-500 a,b) and CMG-900 (c,d) samples.

For the CMG-500 sample, LPH remains consistent for both measurement temperatures, exhibiting a small maximum at ≈10 kPa and decreasing steadily with increasing pressure. The maximum LPH for the CMG-900 sample occurs at ≈20 kPa, with a less significant extent for the higher temperature (40 °C) compared to the 25 °C measurements, indicating milder diffusion restrictions. Beyond 20 kPa, the LPH decreases steadily, as in the case of the CMG-500. It is essential to note that kinetic restrictions can manifest even at elevated measurement temperatures, aligning with findings in other studies. For instance, in

Table 4. Data derived from N_2/−196 °C, Ar/−196 °C, −186 °C, and CO_2/25 °C sorption on CMG-500 and CMG-900 samples outgassed at 300 °C.

Sample	V_{micro} [a]	V_{meso} [b]	$V_{0.016}$ [c]	$V_{0.1}$ [d]	$V_{0.85}$ [e]	$V_{0.85\text{-}0.1}$ [f]
	[$cm^3\ g^{-1}$]					
CMG-500 (N_2, −196 °C)	0.000	0.071	–	0.016	0.068	0.052
CMG-500 (Ar, −196 °C)	–	–	–	0.011	0.033	0.022
CMG-500 (Ar, −186 °C)	0.004	0.107	–	0.052	0.109	0.057
CMG-500 (CO_2, 25 °C)	–	–	0.070	–	–	–
CMG-900 (N_2, −196 °C)	0.100	0.073	–	0.123	0.173	0.050
CMG-900 (Ar, −196 °C)	–	–	–	0.161	0.191	0.030
CMG-900 (Ar, −186 °C)	0.178	0.034	–	0.176	0.211	0.035
CMG-900 (CO_2, 25 °C)	–	–	0.102	–	–	–

[a] Micropore volume calculated by the QSDFT adsorption kernel assuming cylindrical pore geometry; [b] Mesopore volume calculated by the QSDFT adsorption kernel assuming cylindrical pore geometry; [c] Volume adsorbed at 0.016 p/p_0; [d] Volume adsorbed at 0.1 p/p_0; [e] Volume adsorbed at 0.85 p/p_0; [f] The volume representing differences in volumes adsorbed between 0.85 and 0.1 p/p_0.

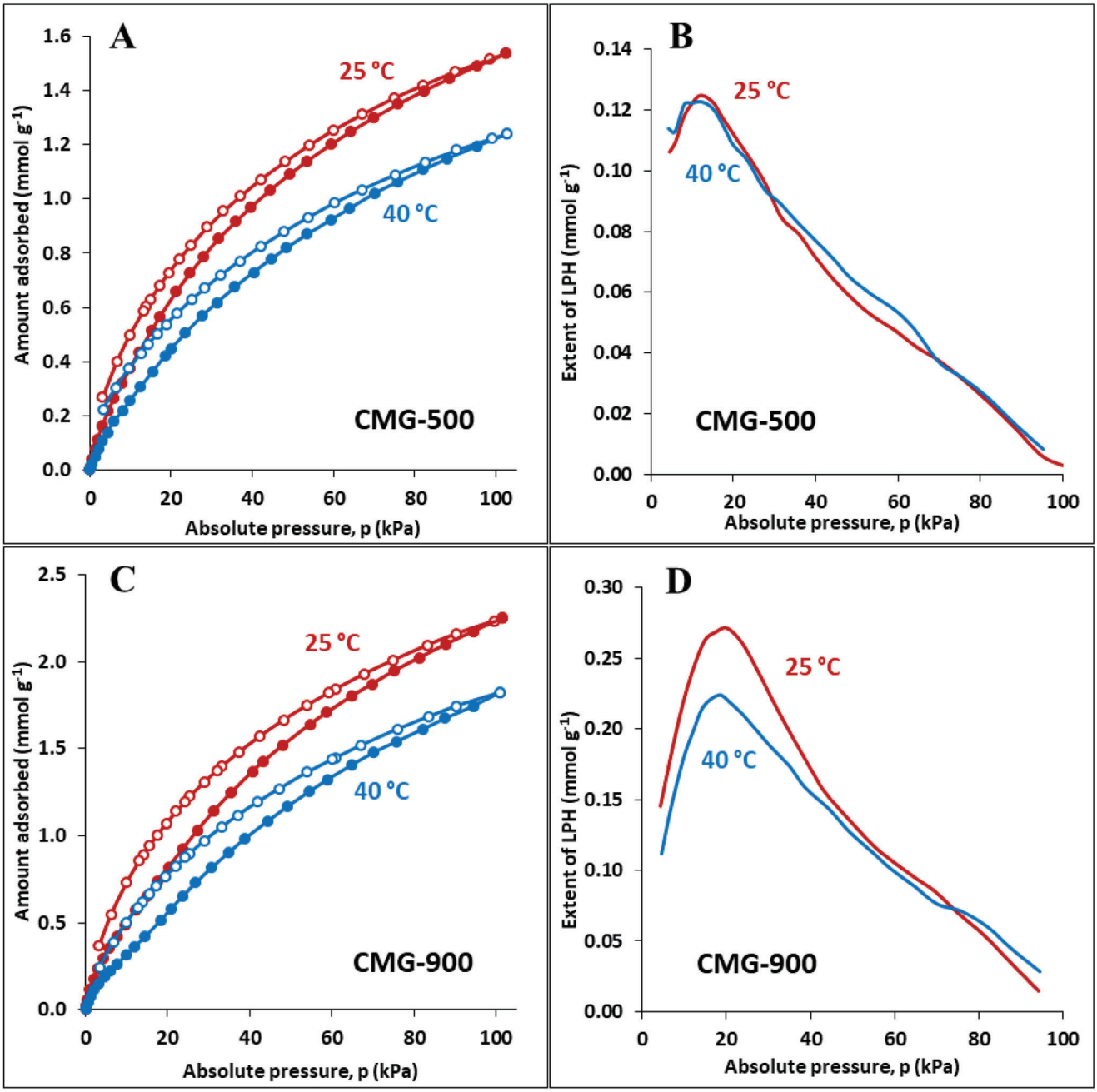

Figure 11. Adsorption–desorption isotherms of CO_2 at 25 and 40 °C a,c) and corresponding extents of LPH b,d) for the CMG-500 and the CMG-900 samples.

ref., [17] authors analyzed ultramicroporous carbons using CO_2 adsorption at 0 and 25 °C, encountering similar kinetic limitations. We demonstrate that even under stringent equilibration criteria, adsorption equilibrium may not be achieved if the porous system is poorly accessible to adsorbate molecules.

3. Conclusion

Our study contributes insights into the complex phenomenon of LPH through a comprehensive analysis of five carbon materials differing in porosity and nature of surface chemistry.

For the STR sample (as-synthesized resorcinol-formaldehyde-based carbon), the extent of LPH remains unchanged, whether the sample is in powder or monolith form. This leads to the conclusion that LPH is not significantly influenced by the physical state of the sample, at least for CO_2 at 25 °C.

The adsorption temperature for the oxidized STR reduces the extent of LPH for CO_2 isotherm at higher adsorption temperatures (5 °C vs 25 °C), aligning with the minimization of kinetic limitations.

An essential aspect highlighted in our study is the critical role of outgassing temperature, particularly for post-synthetically

oxidized samples (for the oxidized STR, in our case). Insufficient outgassing temperature can lead to unreliable experimental data burdened with LPH and strongly underestimated textural properties, especially because of blocking the porosity by substances such as moisture. We propose the use of the highest possible outgassing temperature, as long as there is no concurrent reduction in textural parameters. This recommendation holds, even if it involves the removal of surface groups, to ensure reliability in the results. We propose, especially for treated (e.g., oxidized) samples, performing the outgassing – wetting – re-outgassing experiment to determine whether the increase in adsorbed volume is due to the incomplete removal of pore water or the decomposition of oxygen-containing groups. Conversely, in samples where heteroatoms play a stabilizing role in the texture, such as natural coals, their thermal degradation may occur. However, our study acknowledges the challenges posed by elevated temperatures, especially for thermally unstable samples, necessitating careful consideration of the optimal drying temperature. Therefore, further research in this field is worthwhile.

In CMG samples, the presence of LPH is likely unrelated to their flexibility during CO_2 sorption as revealed by thermomechanical analysis. However, the results of Ar and N_2 adsorption and desorption at cryogenic temperatures strongly indicate that LPH is attributed to kinetic limitations. Interestingly, these limitations persist even during CO_2 adsorption and desorption at elevated temperatures (25 and 40 °C). The kinetic restrictions are more significant for the CMG-500 sample, whereas milder limitations were observed for the CMG-900 sample.

In conclusion, our research hopefully endeavors to contribute insights into the diverse factors affecting LPH, offering practical recommendations for sample preparation and analysis. The study emphasizes the importance of thoughtful consideration in experimental design and proposes avenues for further research in this complex field.

4. Experimental Section

Samples: The synthesis of the STR sample followed the process detailed in,[31] where it is denoted as ST/R 1:1. The material was prepared by combining sol-gel and soft-templating methodologies utilizing resorcinol and formaldehyde precursors. Pyrolysis took place at a target temperature of 500 °C. The production yield was 30.0 wt. %. The resulting carbons were prepared in the monolithic form with hierarchical porosity (containing micro-, meso-, and macropores) and denoted as STR.

The synthesis procedures of the samples are described in Electronic Supplementary Information. The synthesis of CMG samples followed the process detailed in[32] The materials were derived from a microcrystalline cellulose precursor subjected to an ice-templating process. The gel was pyrolyzed at a target temperature of 500 or 900 °C. The production yield was 21.7 and 19.6 wt.%, respectively. The resulting monolithic carbons were denoted as CMG-500 and CMG-900, respectively.

The post-synthetically oxidized variant of the STR sample was prepared by oxidation of a monolithic STR sample in a mixture of nitric acid and hydrogen peroxide, as described in[33] The resulting oxidized hierarchically porous carbon monolith was denoted as STR-ox.

In order to highlight challenges in delicate balancing the removal of substances blocking the porosity, reducing LPH, and preserving the sample's texture, a sample of lignite (natural low-rank coal) in the size fraction of 0.06 – 0.15 mm was used in sub-Section 2.3. The sample was taken from the South Moravian Basin, and selected basic characteristics (e.g., ash content and elemental composition) of this lignite are documented.[34]

Methods: Nitrogen (−196 °C) and argon at (−196, −186 °C) physisorption experiments were performed using a static manometric device (Autosorb iQ-XR, Quantachrome Instruments) in a way described in refs. [35–37] Before the physisorption measurements, samples were outgassed under ultra-high vacuum (UHV) at a final demanded temperature ranging from 60 to 350 °C. The criteria for equilibration were set as follows. The system was considered to be at equilibrium when pressure changes were less than 0.0008 atm (≈81.06 Pa) over a predefined period. This period was set at 8 min for $p/p_0 < 0.01$ points and 5 min for $p/p_0 > 0.01$ points. The volume of micropores and mesopores (V_{micro}, V_{meso}) were calculated from the pore size distribution curves (PSDs) obtained by fitting nitrogen adsorption isotherms (in the range of ≈0.1 – 1 p/p_0) by a hybrid QSDFT adsorption kernel assuming slit-shaped micropores and cylindrical mesopores (Table 2 and Table 3). In Table 4, the QSDFT adsorption kernel assuming cylindrical pore geometry was used for the calculation of V_{micro} and V_{meso}. Liquid volume adsorbed at 0.1 p/p_0 ($V_{0.1}$, roughly representing micropore volume) and 0.85 p/p_0 ($V_{0.85}$, partially representing the sum of micropore and partially mesopore volume). Parameter $V_{0.85\text{-}0.1}$ represents the partial volume of mesopores. Adsorbed and desorbed volumes of liquid nitrogen (−196 °C), argon (−196 °C), and argon (−186 °C) were calculated using liquid densities of 0.806, 1.450, and 1.400 g cm^{-3}, respectively (data available in Quantachrome ASiQwin software v.5.21).

Carbon dioxide sorption experiments were performed in manometric equipment designed and constructed by the LMA group, and are now commercialized by G2mTech Corp. Before the adsorption measurements, samples were outgassed under ultra-high vacuum (UHV) conditions at 150 °C for 8 h. The criteria for equilibration were set as follows. The system was considered to be at equilibrium when pressure changes were less than 0.005 torr min^{-1} (≈1.07 Pa min^{-1}). This is the most stringent criterion that is technically achievable on a given instrument. Liquid adsorbed volume was estimated from $4.29 \cdot 10^{-6}$ to $1.6 \cdot 10^{-2}$ p/p_0, and under the assumption that the CO_2 is filling the pores as a liquid with estimated densities of 1.023 cm^3 g^{-1} (0 °C) and 0.97 cm^3 g^{-1} (25 °C).[17] Normalization of pressure data (p_{norm}) for Figures S5 and S6 (Supporting Information) was done as $p_{norm} = (p - p_{min})/(p_{max} - p_{min})$, where p is absolute pressure, p_{min} and p_{max} refer to minimal and maximal pressures, respectively.

To quantify the LPH, i.e., a degree of disproportion between adsorption and desorption isotherms of N_2, Ar, or CO_2, the parameter called the *extent of LPH* (in cm^3 g^{-1}) was proposed. The extent of LPH was determined as a difference between the adsorbed and the desorbed volume at the given relative pressure (p/p_0). Since the points of adsorption and desorption isotherms did not lie at the same relative pressure, polynomial interpolation was employed to estimate the desorbed volume at the recorded adsorption p/p_0.[38]

To assess the flexibility, involving contractions and expansions of the CMG-500, CMG-900, and the STR-ox samples during CO_2 adsorption, thermomechanical analysis (TMA, Setsys system equipped with a thermomechanical module, Setaram) was employed. The samples were analyzed in the form of monolithic discs with dimensions of ≈3–4 mm in diameter and 1–2 mm in height. A flat measuring probe with a load of 5 g was utilized to monitor the dimensional changes (flexibility) of the samples. Before the TMA measurement, the samples underwent in-situ drying (30 min at 300 °C, heating rate 10 °C min^{-1}) followed by equilibration at 15 °C in an inert Ar environment at a flow rate of 20 ml min^{-1} for 1 h. Subsequently, CO_2 was added to the flow of Ar for 1 h (12 ml min^{-1} for CO_2 and 20 ml min^{-1} for Ar). After completing the adsorption, the sample remained in the Ar flow (20 ml min^{-1}) to desorb adsorbed CO_2. The whole adsorption/desorption cycle was performed at the constant temperature of 15 °C, which is the technically lowest stable temperature.

To analyze the effect of outgassing of STR and STR-ox samples performed prior to gas physisorption measurement, the thermoanalytical measurements (TG-MS) were performed. TG-MS experiments were conducted using the SetsysEvolution instrument (Setaram) directly coupled with a mass spectrometer QMG700 (Pfeiffer) by a SuperSonic system (Setaram). TG-MS curves were recorded with 12–16 mg of the sample (in α-Al_2O_3 crucible) under an argon atmosphere (flow rate 20 ml min^{-1}) up to 350 °C (heating rate 10 °C min^{-1}). The MS signals with $m/z = 2$, 12, 14, 15, 16, 17, 18, 28, 30, 32, and 44 were recorded in MID mode. The selection of

detected gases was based on the prediction of possible gases that could evolve from the decomposition of surface groups of the STR-ox sample.

The surface chemistry of the modified samples was also analyzed using X-ray photoelectron spectroscopy (XPS). XPS analysis was performed in a fully automated Thermo-Scientific K-Alpha spectrometer (pressure 5.10^{-7} Pa). The spectra were collected using Al-K radiation (1486.6 eV), monochromatized by a thin crystal monochromator, generating a focused X-ray elliptical-shaped spot with a major axis length of 400 nm at 3 mA x 12 kV. The CH_x in carbon 1's core level was used as a reference binding energy (284.6 eV).

Supporting Information

Supporting Information is available from the Wiley Online Library or from the author.

Acknowledgements

This work was supported by the projects: LUASK22049 (INTER-EXCELLENCE II, MŠMT), APVV SK-CZ-RD-21–0068, and SGS16/PřF/2022. The Czech team (V.S.) was supported by the European Union under the LERCO project number CZ.10.03.01/00/22_003/0000003. J.S.A. would like to acknowledge financial support from MINECO (PID2022-142960OB-C21) and MCIN/AEI/10.13039/501100011033 and EU "NextGeneration/PRTR" (Project PCI2020-111968/ERANET-M/3D-Photocat), EU MSCA project CLEANWATER (Grant Agreement: 101131382), and Conselleria de Innovación, Universidades, Ciencia y Sociedad Digital (Project CIPROM/2021/022).

Open access publishing facilitated by Ostravska univerzita, as part of the Wiley - CzechELib agreement.

Conflict of Interest

The authors declare no conflict of interest.

Data Availability Statement

The data that support the findings of this study are available from the corresponding author upon reasonable request.

Keywords

artificial hysteresis, degassing, diffusion limitations, open isotherms, oxidized carbon

Received: December 21, 2023
Revised: April 8, 2024
Published online:

[1] M. Thommes, K. Kaneko, A. V. Neimark, J. P. Olivier, F. Rodriguez-Reinoso, J. Rouquerol, K. S. W. Sing, *Pure Appl. Chem.* **2015**, *87*, 1051.
[2] T. Zelenka, T. Horikawa, D. D. Do, *Adv. Colloid Interface Sci.* **2023**, *311*, 102831.
[3] P. Maziarka, C. Wurzer, P. J. Arauzo, A. Dieguez-Alonso, O. Mašek, F. Ronsse, *Chem. Eng. J.* **2021**, *418*, 129234.
[4] W. Lai, S. Yang, Y. Jiang, F. Zhao, Z. Li, B. Zaman, M. Fayaz, X. Li, Y. Chen, *Adsorption* **2020**, *26*, 633.
[5] C. Balzer, R. T. Cimino, G. Y. Gor, A. V. Neimark, G. Reichenauer, *Langmuir* **2016**, *32*, 8265.
[6] C. Balzer, S. Braxmeier, A. V. Neimark, G. Reichenauer, *Langmuir* **2015**, *31*, 12512.
[7] A. M. Silvestre-Albero, J. M. Juárez-Galán, J. Silvestre-Albero, F. Rodríguez-Reinoso, *J. Phys. Chem. C* **2012**, *116*, 16652.
[8] V. Yu. Yakovlev, A. A. Fomkin, A. V. Tvardovski, *J. Colloid Interface Sci.* **2003**, *268*, 33.
[9] V. Yu. Yakovlev, A. A. Fomkin, A. V. Tvardovski, *J. Colloid Interface Sci.* **2004**, *280*, 305.
[10] H. Wu, C. G. Thibault, H. Wang, K. A. Cychosz, M. Thommes, J. Li, *Microporous Mesoporous Mater.* **2016**, *219*, 186.
[11] C. Reichenbach, G. Kalies, J. Lincke, D. Lässig, H. Krautscheid, J. Moellmer, M. Thommes, *Microporous Mesoporous Mater.* **2011**, *142*, 592.
[12] J. Lincke, D. Lässig, J. Moellmer, C. Reichenbach, A. Puls, A. Moeller, R. Gläser, G. Kalies, R. Staudt, H. Krautscheid, *Microporous Mesoporous Mater.* **2011**, *142*, 62.
[13] G. Kyriakou, C. R. Theocharis, *Studies in Surface Science and Catalysis*, Elsevier, Amsterdam **2002**.
[14] C. Reichenbach, D. Enke, J. Möllmer, D. Klank, M. Klauck, G. Kalies, *Microporous Mesoporous Mater.* **2013**, *181*, 68.
[15] S. Sircar, H. Wu, J. Li, A. D. Lueking, *Langmuir* **2011**, *27*, 14169.
[16] F. Rouquerol, J. Rouquerol, K. S. W. Sing, P. L. Llewellyn, G. Maurin, *Adsorption by Powders and Porous Solids: Principles, Methodology and Applications*, Elsevier/AP, Amsterdam **2014**.
[17] R. V. R. A. Rios, J. Silvestre-Albero, A. Sepúlveda-Escribano, M. Molina-Sabio, F. Rodríguez-Reinoso, *J. Phys. Chem. C* **2007**, *111*, 3803.
[18] S. J. Gregg, K. S. W. Sing, *Adsorption, Surface Area, and Porosity*, Academic Press, London/New York **1982**.
[19] A. H. Farmahini, K. Limbada, L. Sarkisov, *Adsorption* **2022**, *28*, 219.
[20] G. Hotová, V. Slovák, O. S. G. P. Soares, J. L. Figueiredo, M. F. R. Pereira, *Carbon* **2018**, *134*, 255.
[21] R. M. Fakoussa, Hofrichter M, Appl Microbiol Biotechnol. 1999, 52, 25.
[22] S. Deevi, E. Suuberg, *Fuel* **1987**, *66*, 454.
[23] T. Zelenka, B. Taraba, *Int. J. Coal Geol.* **2014**, *132*, 1.
[24] S. Lowell, J. E. Shields, M. A. Thomas, M. Thommes, *Characterization of Porous Solids and Powders: Surface Area, Pore Size and Density*, Springer, Netherlands **2006**.
[25] M. Thommes, K. A. Cychosz, *Adsorption* **2014**, *20*, 233.
[26] A. Figini-Albisetti, L. F. Velasco, J. B. Parra, C. O. Ania, *Appl. Surf. Sci.* **2010**, *256*, 5182.
[27] L. F. Velasco, A. Devos, P. Lodewyckx, *Carbon* **2019**, *152*, 409.
[28] B. McEnaney, *J. Chem. Soc., Faraday Trans. 1* **1974**, *70*, 84.
[29] H. Huang, W. Zhang, D. Liu, B. Liu, G. Chen, C. Zhong, *Chem. Eng. Sci.* **2011**, *66*, 6297.
[30] J. Silvestre-Albero, A. Silvestre-Albero, F. Rodríguez-Reinoso, M. Thommes, *Carbon* **2012**, *50*, 3128.
[31] P. Bulavová, J. Parmentier, V. Slovák, *Microporous Mesoporous Mater.* **2018**, *272*, 155.
[32] A. Kryeziu, V. Slovak, J. Parmentier, T. Zelenka, S. Rigolet, *Ind. Crops Prod.* **2022**, *183*, 114961.
[33] G. Hotová, V. Slovák, *Anal. Chem.* **2017**, *89*, 1710.
[34] B. Taraba, T. Zelenka, *J. Therm. Anal. Calorim.* **2017**, *128*, 1505.
[35] G. Zelenková, T. Zelenka, V. Slovák, *Microporous Mesoporous Mater.* **2021**, *326*, 111358.
[36] M. Almáši, A. Sharma, T. Zelenka, *Inorg. Chim. Acta* **2021**, *526*, 120505.
[37] T. Zelenka, K. Simanova, R. Saini, G. Zelenkova, S. P. Nehra, A. Sharma, M. Almasi, *Sci. Rep.* **2022**, *12*, 17366.
[38] T. Zelenka, *Microporous Mesoporous Mater.* **2016**, *227*, 202.